Soft Matter

Accepted Manuscript

ROYAL SOCIETY OF CHEMISTRY

www.rsc.org/softmatter

1

Simulation of the tensile properties of silica aerogels: the effects of cluster structure and primary particle size

Qiang Liu[a], Zixing Lu[a], Zijun Hu[b], Junning Li[b], Man Zhu[a], Zeshuai Yuan[a], ZhenyuYang[a]

Abstract: A new two-level model is proposed to investigate the relationship between the mechanical properties and microstructure of silica aerogels. This two-level model consists of the particle-particle interaction model and cluster structure model. The particle-particle interaction model is proposed to describe interactions between primary particles, in which the polymerization reaction between primary particles is considered. The cluster structure model represents the geometrical structure of silica aerogels, and it is established using a modified diffusion-limited colloid aggregation (DLCA) algorithm. This two-level model is used to investigate the tensile behavior of silica aerogels based on discrete element method (DEM). The numerical results show that primary particle size has significant effects on the elastic modulus and tensile strength properties of silica aerogels. Moreover, the power-law relationships between tensile properties and aerogel density are dependent on the variation of primary particle radius with density. The present results can explain the difference among different experimental exponents to a certain extent. In comparison with experimental data within a wide density range, this two-level model provides good quantitative estimations of the elastic modulus and tensile strength of silica aerogels after size effects of primary particle are considered. This paper provides a fundamental understanding of the relationship between the mechanical properties and

[a] *Institute of Solid Mechanics, Beihang University, Beijing, 100191, China*
Email: luzixing@buaa.edu.cn ; Tel.: +86 10 82315707; Fax: +86 10 82318501
[b] *National Key Laboratory of Advanced Functional Composite Material Technology, Beijing, 100076, China*

microstructure of silica aerogels. The two-level model can be extended to study the mechanical properties of other aerogels and aerogel composites.

Keywords: silica aerogels, two-level model, size effects, tensile strength, DEM.

Introduction

As a type of ultra-light nanoporous materials, aerogels were firstly introduced by Kistler in 1931.[1] These materials are the three-dimensional assemblies of nanoparticles and have a pearl-necklace network structure.[2, 3] Silica aerogels are the best studied of these materials, and exhibit many extraordinary properties, such as high specific surface area, high porosity, low thermal conductivities, low dielectric constants, and high acoustic attenuations.[4-6] Therefore, silica aerogels are of great interest for many applications including thermal and acoustic insulation, optics, catalysis, and chromatographic systems. However, these potential applications have been restricted due to the poor mechanical properties and extreme fragility of silica aerogels.[7] To improve the mechanical properties, it is therefore essential to study the relationship between the mechanical properties and microstructure of silica aerogels.

The microstructure of silica aerogels is often described as the fractal assemblies of amorphous silica nanoparticles based on experiments, through which a mass-fractal character has been verified.[8, 9] Therefore, the relationship between the mechanical properties and microstructure of silica aerogels is different from that predicted by Gibson and Ashby model[10] used for foam-like materials. For example, the power-law exponents in 'elastic modulus-density' (modulus-density) relationship is between 3 and 4 for silica aerogels,[11-13] while this value is 2 in Gibson and Ashby model. In the

3

work of Ma *et al.*,[14] the large power-law exponent of silica aerogels was explained by the variation of structural connectivity with density. Based on this viewpoint, the poor mechanical properties of low density silica aerogels are due to the high ratio of dangling particle chains in microstructure.

Up to now, the structure-property studies of silica aerogels are still limited due to the restriction of experimental techniques. Therefore, computational simulation has been widely employed to study the relationship between the mechanical properties and microstructure of silica aerogels. Several atomistic models have been proposed to simulate the nanoporous structure of silica aerogels.[15-18] In these atomistic models, the nanoporous structure was obtained by scaling the simulation box[15-18] of dense amorphous silica, or charge scaling method[17] using molecular dynamics (MD) simulation. These atomistic models are valid to predict the fractal dimension and modulus-density relationship of silica aerogels. However, there are two drawbacks in atomistic models. Firstly, the nanoporous structure with uniformly distributed pores is some different from that observed by experiments.[19] Secondly, the time and length scales are not comparable with experiments due to the computational cost of MD simulation.[20] Therefore, the atomistic models are insufficient to investigate the mechanical properties of silica aerogels at a large scale as indicated by Gelb *et al.*[20]

It is widely accepted that silica aerogels consist of nanometer-sized particles, including the primary particles at several nanometer scale and secondary particles at tens of nanometer scale.[6] Primary particles are often considered as dense amorphous silica while secondary particles are the effective particles consisted of primary

4

particles. Therefore, at a larger scale, silica aerogels are considered as the aggregation

of nanoparticles, or called cluster structure. Due to this fact, some numerical models

based on particle aggregation algorithm are proposed to describe the microstructure of

silica aerogels. These particle aggregation algorithms generally include the

diffusion-limited aggregation, reaction-limited aggregation, diffusion-limited cluster

aggregation, and reaction-limited cluster aggregation.[20, 21] In these algorithms, DLCA

algorithm is the most widely adopted, and the corresponding model sufficiently

describe the structural feature of silica aerogels.[22] Strictly speaking, the models

generated by DLCA algorithm cannot be directly used to simulate the mechanical

properties of silica aerogels because the particles in these models are rigid.[20] To solve

this problem, Ma *et al*.[23] adopted finite element (FE) method to predict the power-law

relationship between the elastic modulus and relative density of silica aerogels. In

their model, the cluster structure was generated by combining DLCA algorithm with

the dangling bond deflection mechanism;[24] the cluster structure was then transformed

into beam networks by connecting the centers of contacting particles; for beam

elements, the elastic modulus was set to be an arbitrary value, and the radius to be 0.2

in units of particle size; the relative elastic modulus of beam networks was calculated

using FE method, and considered as that of silica aerogels. Similarly, Barbero *et al*.[25]

generated a FE model based on reaction-limited cluster aggregation algorithm, in

which primary particles are represented by solid elements.

These FE models based on particle aggregation algorithm provide alternative

approach to the relative elastic properties of silica aerogels. However, in these FE

5

models, the material parameters are not the true ones of primary or secondary particles. In other words, the mentioned FE models cannot be directly used for quantitative estimation of the mechanical properties for silica aerogels. Therefore, several multi-scale models are proposed to solve this problem. In these multi-scale models, the particles' properties are obtained by MD simulation or theoretical analysis. Gelb et al.[26, 27] adopted three empirical potentials to describe the interactions between primary particles, and then investigated the elastic properties of silica aerogels using MD simulation. Different from work of Gelb et al., silica aerogels were idealized as cubic arrays of secondary particles in the work of Lei et al.[28] In their two-level model, the properties of secondary particles are obtained by MD simulation, and the elastic properties of cubic arrays are derived based on theoretical derivations. Compared with atomistic models and FE models, multi-scale models are more effective in balancing the computational cost and accuracy of quantitative estimation.

In a word, the aforementioned models are verified to be valid for predicting the elastic properties of silica aerogels. In contrast, these models are not used to predict the strength properties except the model of Murillo et al.;[18] however, significant quantitative deviation is observed between the numerical results of Murillo et al. and experimental data. Besides, the relationship between the mechanical properties and microstructure of silica aerogels has been not well understood. In this paper, we propose a new two-level model to investigate the tensile properties of silica aerogels. This two-level model consists of the particle-particle interaction model and cluster structure model. The former is used to describe interactions between primary particles

6

based on theoretical derivations. The latter is used to represent the cluster structure based on a modified DLCA algorithm using DEM simulation. The elastic modulus and tensile strength of silica aerogels are then predicted using DEM by introducing the particle-particle interaction model into cluster structure model. Moreover, the influences of cluster structure and primary particle size on the tensile properties and power-law relationships of silica aerogels are discussed. Some key conclusions are drawn in the final section.

Model description

Particle-particle interaction model

The basic particles in our model are primary particles of silica aerogels, and their properties are assumed to be same as those of dense amorphous silica. The primary particle size is dependent on sol-gel process, and found to be in the range of 2-7nm in diameter.[6, 29] To facilitate analysis, we assume all primary particles have uniform radius R as literature.[22, 24, 26] The primary particle radius can be approximately estimated by the specific surface area S_C of silica aerogels,[29] i.e.

$$R = \frac{3 \times 10^3}{\rho_s S_c} \tag{1}$$

Where ρ_s is the density of primary particles, and taken as $2.2 \, g \cdot cm^{-3}$. In Eq. (1), R has the unit of nanometer (nm).

Clearly, the size of bonds or necks between primary particles has significant effects on the mechanical properties of silica aerogels. It is believed that the attachment between primary particles is through the formation of Si-O-Si bonds in the

sol-gel process; however, the conversion of primary particles (sols) to a gel is not easily understood.[29] In some previous researches,[23, 30] the relative neck radius a_0^* ($a_0^*=a_0/R$ and a_0 is the neck radius) was taken as a constant value to estimate the mechanical properties of silica aerogels. Nevertheless, experimental results show a tendency toward higher a_0^* at smaller primary particle size; for example, the microstructure is better described as a fiber-like network rather than a series of independent particles for the silica aerogels with small primary particle size.[29] Therefore, a_0^* should change with primary particle size. Iler[29] estimated the size-dependent a_0^* by considering the transport and re-deposition of silica. However, the a_0^* obtained by Iler's model overestimates neck size because the true aging process of silica aerogels is not so completed as assumed in Iler's model.[30]

In this paper, we adopt a simplified method to estimate the size-dependent a_0^*. As shown in Fig. 1, the formation of interparticle neck is considered to be caused by the reduction of free surface; the status of two primary particles changes from Fig. 1(a) to Fig.1(c) through the polymerization reaction, i.e.

$$\equiv \text{Si-OH} + \text{HO-Si} \equiv \ \rightarrow \ \equiv \text{Si-O-Si} \equiv \ + \text{H}_2\text{O} \tag{2}$$
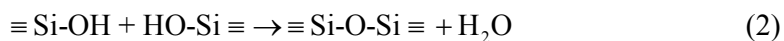
From the status of Fig. 1(a) to that of Fig. 1(c), the loss in energy mainly includes two parts: one is the Si-OH surface energy; the other is H-OH bond energy in H_2O. Therefore, from the view of energy conservation, the formation of interparticle neck is better described from Fig. 1(b) to Fig. 1(c). As the surface energy of amorphous SiO_2 surface is much larger than that of Si-OH surface, we can consider the mixed free surface in Fig. 1(b) as an effective surface following Schwarz:[31] the surface energy of

8

the effective surface (γ_{eff}) is separated into the short-range component (γ_1) and

long-range component (γ_2), i.e.

$$\gamma_{eff} = \gamma_1 + \gamma_2 \tag{3}$$

Clearly, the short-range component is mainly determined by the surface energy of

amorphous SiO_2 surface while the long-range component is governed by the surface

energy of Si-OH surface. Here, γ_1 and γ_2 are respectively taken as

$$\gamma_1 = \gamma_{SiO_2} - \gamma_{Si-OH}^{liquid} \tag{4}$$

$$\gamma_2 = \gamma_{Si-OH}^{liquid} \tag{5}$$

In the two equations, γ_{SiO_2}, γ_{Si-OH}^{liquid} are the surface energy of amorphous SiO_2 surface

and Si-OH surface in solution, respectively. It is deduced that γ_{eff} and γ_{SiO_2} are

equal in value by substituting Eq. (4) and Eq. (5) into Eq. (3); however, γ_{eff} and

γ_{SiO_2} have different short-range and long-range components. Therefore, γ_{eff} is

actually different from γ_{SiO_2}. The validity of Eq. (4) and Eq. (5) is guaranteed by the

condition that γ_{SiO_2} is much larger than γ_{Si-OH}^{liquid}. Similar to Ref. 29, the adhesion

between primary particles is assumed to occur when primary particles collide. The

adhesion work w_{ad} also includes two components, i.e.

$$w_{ad} = 2\gamma_{eff} = 2\gamma_1 + 2\gamma_2 \tag{6}$$

Therefore, according to the model of Schwarz[31] modified from Johnson *et al.*,[32] the

contact area between two primary particles is expressed as

$$a_0 = (\frac{R}{K})^{1/3}(\sqrt{F_H} + \sqrt{3\pi R w_{ad} - 3F_H})^{2/3} \tag{7}$$

Here, K is the effective elastic modulus of primary particles and expressed as

$K = 4E_0/3(1-\mu_0^2)$ (E_0 and μ_0 are the elastic modulus and Poisson's ratio of

primary particles); F_H represents the adhesion force between primary particles, i.e.

$$F_H = \frac{3}{2}\pi R \gamma_1 + 2\pi R \gamma_2 \tag{8}$$

We assume that the polymerization reaction between two primary particles occurs in the contact area determined by Eq. (7), and a_0 is considered as the final neck radius. Substituting Eq. (4)-(6) and Eq. (8) into Eq. (7), we express the neck radius a_0 as

$$a_0 = \left(\frac{R}{K}\right)^{1/3}\left(\sqrt{\frac{3\pi R}{2}(\gamma_{SiO_2} - \gamma_{Si-OH}^{liquid})} + \sqrt{\frac{\pi R}{2}(3\gamma_{SiO_2} + \gamma_{Si-OH}^{liquid})}\right)^{2/3} \tag{9}$$

γ_{Si-OH}^{liquid} is dependent on the property of the sol-gel solution; therefore, a_0 is determined by the geometrical size and elastic properties of primary particles as well as the property of the sol-gel solution.

In the following, the interactions between primary particles and the deformation mechanism of particle chains will be presented when silica aerogels are subjected to loading. Similarly, the interactions also include short-range and long-range ones as shown in Fig. 2: the short-range interaction is determined by interparticle neck while the long-range interaction is the Van der Waals force dependent on the surface energy of Si-OH surface. In this paper, we assume that silica aerogels are in the condition of dry air; therefore the surface energy of Si-OH surface in Fig. 2 is denoted as γ_{Si-OH}^{air}. Generally speaking, silica aerogels are highly porous, and the mean coordination number of primary particle (the number of contact points among a particle and its neighbors) is about 3 according to experimental results.[30] Therefore, bending is the main deformation mechanism of particle chains. To facilitate analysis, the particle chain's stiffness is assumed to be determined by short-range interaction while the

particle chain's strength is governed by both short-range and long-range interactions.

Although the Hertzian elastic contact theory is based on continuum mechanics, it has been verified to be valid in nano-scale by MD simulation.[33, 34] Thus the Hertzian elastic contact theory is widely adopted to describe the contact at nano-scale.[33-35] In this paper, a modified elastic contact theory is employed to analyze the short-range interaction. As hinted earlier, the neck radius a_0 cannot be neglected relative to particle radius. Therefore, the contact model with finite bond size[36, 37] is employed to determine the contact stiffness between primary particles, i.e.

$$k^N = \frac{E_0 a_0}{1 - \mu_0^2} f_N^*(a_0^*, \mu_0) \tag{10}$$

$$k^T = \frac{2E_0}{(2 - \mu_0)(1 + \mu_0)} f_T^*(a_0^*, \mu_0) \tag{11}$$

Where k^N and k^T are the normal and tangential contact stiffness, respectively; $f_N^*(a_0^*, \mu_0)$ and $f_T^*(a_0^*, \mu_0)$ are obtained by FE simulation,[36, 37] which are respectively expressed as

$$f_N^*(a_0^*, \mu_0) = \frac{1 + a_0^*[\frac{\pi}{6}(1 - \mu_0^2)(1 + 2a_0^*) - a_0^*]}{\sqrt{1 - a_0^{*2}} - \frac{1.12 - 0.12\mu_0 + 1.41\mu_0^2 + 1.04\mu_0^4}{\pi} a_0^*[1 + a_0^*[\frac{\pi}{6}(1 - \mu_0^2)(1 + 2a_0^*) - a_0^*]]} \tag{12}$$

$$f_T^*(a_0^*, \mu_0) = \frac{1 + a_0^{*2}[\frac{\pi}{6}(1 - \mu_0^2)(1 + 2a_0^*) - a_0^*]}{\sqrt{1 - a_0^{*2}}} \tag{13}$$

Based on elastic contact mechanics, the normal force F_N and tangential force F_T between primary particles are given as

$$F_N = k^N u^N, \quad F_T = k^T u^T \tag{14}$$

Where u^N and u^T are the translational displacements in normal and tangential directions, respectively. The normal and tangential resisting moments (M_N and

---

11

M_T) are obtained by

$$M_N = -\overline{k^T} J \cdot \theta^N, \qquad M_T = -\overline{k^N} I \cdot \theta^T \tag{15}$$

Where $J = \pi a_0^4 / 2$ and $I = \pi a_0^4 / 4$; $\overline{k^N} = k^N / \pi a_0^2$ and $\overline{k^T} = k^T / \pi a_0^2$; θ^N and

θ^T are the accumulated relative rotations along the normal and tangential axis of

interparticle neck, respectively. The maximum tensile and shear stress (σ_{max} and

τ_{max}) acting on interparticle neck are calculated according to the beam theory,[38, 39] i.e.

$$\sigma_{max} = -\frac{F_N}{\pi a_0^2} + \frac{|M_T|}{I} a_0 \tag{16}$$

$$\tau_{max} = \frac{|F_T|}{\pi a_0^2} + \frac{|M_T|}{J} a_0 \tag{17}$$

It is important to note that $F_N > 0$ represents compressive load in Eq. (16).

The fracture of interparticle neck occurs due to tensile, shear or bending

deformation of particle chains. In this paper, the maximum principle stress is used to

identify the fracture of interparticle neck (or debonding), which is evaluated by

$$\sigma_1 = \sqrt{\sigma_{max}^2 + 4\tau_{max}^2} \tag{18}$$

Here, we employ the adhesive model of Schwarz[31] to determine the critical pull-off

force between two contacting primary particles. The pull-off force should be

dependent on both the short-range and long-range interactions, i.e.

$$F_C = \frac{3}{2}\pi R(\gamma_{SiO_2} - \gamma_{Si-OH}^{air}) + 2\pi R\gamma_{Si-OH}^{air} \tag{19}$$

The critical stress on the neck (σ_C) is evaluated by the pull-off force with

$\sigma_C = F_C / \pi a_0^2$. Therefore, the fracture of interparticle neck occurs when $\sigma_1 \geq \sigma_c$.

Cluster structure model

In this paper, the microstructure of silica aerogels is generated by a modified DLCA algorithm based on Ref. 24, in which the dangling bond deflection mechanism was considered. Different from Ref. 24, the present DLCA algorithm is performed using DEM software PFC3D.[40] This computational tool has been widely used to investigate the mechanical properties of particle system[37-39], and perform the coarse-grained simulation of carbon nanotubes[41]. Therefore, the basic particles are flexible particles in the present DLCA algorithm. That is, the move of particles and clusters are realized by solving the motion equations of particles, but not picking up a cluster according to a defined probability function as introduced in the literature.[24]

It is noteworthy that the neck area is taken as $a_{gel} = a_0 / 2$ to perform DLCA algorithm. This is due to the fact that polymerization reaction is not fully completed during the gel formation, The present cluster structure model is established as follows. Firstly, particles are placed in the simulation box as the cubic array configuration; the properties of particles and interparticle necks are determined by substituting a_{gel} into Eq. (10)-Eq. (13) and Eq. (19). Secondly, each particle is assigned a velocity with random direction. Thirdly, the motion and collision of particles are simulated using DEM, during which the wall boundary condition is adopted; the wall boundaries reflect the particles which attempt to move through boundaries. Next, any two contacting particles are connected by a bond; the bond creation is terminated until a single-connected cluster is obtained (gel structure). Meanwhile, the dangling bond deflection mechanism is considered as introduced by Ma *et al.*[24] To simulate the aging

13

process, the neck radius in gel structure a_{gel} is replaced by the a_0, and then the gel structure is fully relaxed. Finally, the cluster structure model representing the microstructure of silica aerogels is established through the above procedure.

Fig. 3 shows a representative cluster structure of silica aerogels, in which the primary particle radius is 2nm and the density (ρ^*) is 0.11 g/cm^3 (with porosity of 95%). The model contains 64000 primary particles, and the model length is up to 350.05nm. By contrast, the model length of the atomistic models used for silica aerogels is generally less than 15nm[15-18]. As shown in Fig. 3(a), the primary particles aggregate into secondary particles, and then these secondary particles further aggregate into the cluster structure of silica aerogels. In Fig. 3(b), a local structure with size of $185 \times 185 \times 80$ nm is cut from Fig. 3(a) to show the porous structure of silica aerogels. Clearly, the pore size is not uniform in the cluster structure; it may reach tens of nanometers among secondary particles, which is consistent with experimental observation. In Fig. 3, the color of primary particles represents their coordination number. In the model with density of 0.11g/cm^3, the coordination number is between 1 and 6, and the mean coordination number is about 3.10. This mean value is close to the one obtained by the model of Gelb et al[26, 27].

Simulation and results

Method

The present two-level model is implemented in DEM in order to gain an insight into the fracture and deformation behavior of silica aerogels. In this paper, we only focus on the tensile behavior of silica aerogels. The simulation scheme is shown in

14

Fig.4, in which a numerical sample is bonded to the boundary particle aggregations. The numerical sample should be under tension when the boundary particle aggregations are applied by tensile displacement w, i.e.

$$w = \frac{1}{2}L\varepsilon_z \qquad (20)$$

Where L is the length of numerical sample and ε_z is tensile strain. The tensile stress of numerical sample is calculated by the out-of-balance force on boundaries, i.e.

$$\sigma_z = \frac{|F_{top} - F_{btm}|}{2L^2} \qquad (21)$$

Where F_{top} and F_{btm} are the total out-of-balance force on the top and bottom boundaries, respectively.

The free boundary is adopted in the non-loading directions when tensile behavior of silica aerogels is simulated. To eliminate the effects of model size, we adopt the model with 64,000 particles in all simulations. In this case, the model size is over 10 times of the mean pore size of silica aerogels, which ensures the corresponding model can represent the microstructure of silica aergoels. In this paper, the material parameters in particle-particle interaction model are obtained using MD simulation. To obtain the material parameters of amorphous silica, we prepare amorphous silica by the melt-quenching method[42] in MD simulation, in which the Morse potential developed by Brommer *et al.*[43] is employed. The elastic parameters of amorphous silica are calculated based on a uniaxial tension or compression simulation, while the surface energy is calculated by the method proposed by Frolov and Mishin.[44] The details are presented in the 'Supplementary Data' file for the MD simulation of

15

amorphous silica. The surface energy of Si-OH surface is cited from the MD

numerical results of Sabine and Martin.[42] Finally, these material parameters used for

the following simulation are summarized in Table 1. The primary particle radius is

approximately determined by the specific surface area of silica aerogels (Eq. (1)),

which will be specified for each case in the following.

Tensile response and microstructure evolution

In this section, the main aim is to present a qualitative description about the

tensile stress-strain response and microstructure evolution of silica aerogels using our

two-level model. Therefore, the numerical results reported here is from one numerical

sample with density of 0.12g/cm^3; however, the quantitative results in the next section

are from 6 different numerical samples. Generally speaking, the specific surface area

is about between 500 and 850 m^2/g for the case of $\rho^* = 0.12 \text{ g/cm}^3$; therefore, the

primary particle radius is taken as 2nm in this model according to Eq. (1).

Fig. 5 shows the variation of stress and the number of fractured necks with strain

obtained by numerical simulation. Starting from point ①, stress increases

continuously to reach point ②. During this process, the number of fractured necks

increases slowly. After that, stress increases slowly until a clear stress drop occurs,

indicating a brittle fracture under tension. Meanwhile, the increasing rate of fractured

necks almost reaches the maximum value. The number of fractured necks is about 125

corresponding to the stress drop, which is only 0.12% of the total necks. After the

stress drop, stress decreases continuously with strain, while the number of fractured

necks increases slowly again. In this paper, the elastic modulus of numerical model is

16

defined as the slope of the linear part of the stress-strain curve, and the tensile strength

is calculated by the maximum stress of the stress-strain curve. For the silica aerogels

with $\rho^* = 0.12 \, \text{g/cm}^3$, numerical results show that the elastic modulus and tensile

stress are about 5.56MPa and 0.081MPa, respectively. It indicates silica aerogels with

low density are extremely fragile. The detailed quantitative comparisons between the

present numerical results and experimental will be in the next section.

Fig. 6 shows the microstructure evolution of silica aerogels, and the four figures

①-④ are corresponding to the four points denoted in Fig. 5, respectively. To facilitate

analysis, the microstructure shown in Fig. 6 is a local configuration with size of

$340 \times 340 \times 80 \, \text{nm}$; the green particles represent the intact particles whose coordination

number does not change during tension, while the red particles are the debonding

particles whose coordination number changes during tension. In the configuration ②

(with tensile strain of ε=1.5%), there are only a few debonding particles. That is, the

main framework of the cluster structure is almost intact. Consequently, the stress still

increase slowly before point ② in Fig. 5. Afterwards, the number of debonding

particles rapidly increase with strain. Especially, many debonding particles are

observed between two clusters (secondary particles); that is, damage extends to the

main framework (configuration ③ in Fig. 6). As a result, the stress drop is observed

in the stress strain curve. After point ③, silica aerogels almost lose the load-bearing

capacity. Therefore, the fractured necks increases slightly while the pores close to the

debonding particles are evidently enlarged (configuration ④ in Fig. 6).

Fig. 5 and Fig. 6 indicate that that the macroscopic failure of silica aerogels is

caused by the increase of debonding particles. In order to investigate the failure

probability of the primary particles at different positions in microstructure, the

debonding particles in Fig. 6(④) are classified by their initial coordination number

(k). As shown in Fig. 7, the initial coordination number of debonding particles

(CNDPs) is mainly between 3 and 4. The probability distribution of CNDPs can be

understood as follows: the primary particles with $k = 1$ or $k = 2$ are mainly located

in the dangling chains; the primary particles with $k = 3$ or $k = 4$ are probably

between different clusters; the primary particles with $k > 4$ are mainly the ones

within clusters. For these debonding particles, they are impossible to be completely

debonded from the main framework. We calculate the variation of coordination

number for each debonding particle (VCNDP), and the probability distribution is also

demonstrated in Fig. 7. The VCNDP result shows that most debonding particles lose

one adjacent primary particle after brittle fracture.

In a word, the tensile fracture of silica aerogels is due to the debonding of the

primary particles locating between different clusters. In other word, it can be

described as the neck fracture between different clusters or secondary particles as

mentioned in some references.[7, 28] According to the CNDPs and VCNDP results, it can

be inferred that the poor mechanical properties of silica aerogels are mainly

determined by the low crosslink density (coordination number) of primary particles.

Discussions

The effect of primary particle size

As mentioned in the work of Iler,[29] the primary particle size is dependent on

18

sol-gel condition. For example, the silica aerogels prepared under basic condition have larger primary particles than those prepared under neutral or acid conditions. Therefore, it is interesting to study the effects of primary particle size on the tensile properties of silica aerogels. In the particle-particle interaction model presented in Section 2, we obtain the size-dependent properties of interparticle neck. Fig. 8(a) shows the effects of particle radius (R) on the neck radius, the normal and tangential contact stiffness and the tensile strength of interparticle necks. Consistent with experimental results, the relative neck radius a_0^* obtained by Eq. (9) reversely decreases with increasing R . a_0^* is up to 0.59 for the case of $R = 1 \, \text{nm}$. In this case, gel structure is better described as a fiber-like network.[29] However, a_0^* is only 0.27 for the case of $R = 10 \, \text{nm}$, which is close to the fitted value (0.25) obtained by Woignier *et al.*[30] In this paper, the contact stiffness of interparticle neck is normalized by R . The k^N/R and k^T/R represent the resistance to elastic deformation of particle chains. In Fig. 8(a), k^N/R and k^T/R both decrease with increasing R . That is, the particle chains with smaller particles are stiffer if their lengths are the same. Similarly, the neck strength σ_C decreases as R increases.

Fig. 8(b) shows the effects of primary particle size on the elastic modulus and tensile strength of silica aerogels. As hinted in Fig. 8(a), particle chains become softer with increasing R ; therefore, the elastic modulus of silica aerogels (particle chain networks) decreases with increasing R . This conclusion was also drawn by Gelb *et al.*[28] Similarly, the silica aerogels with larger primary particles have lower tensile strength due to the lower neck strength. As shown in Fig. 8(a) and Fig. 8(b), the size

effects of primary particles become less evident when R is larger. The size effects obtained from present numerical results are also accordance with experimental results of Woignier et al.,[11] in which the silica aerogels prepared in basic condition had larger primary particles but smaller elastic modulus and tensile strength than those prepared under neutral and acid conditions. Therefore, to a certain extent, the present results account for the effects of pH on the mechanical properties of silica aerogels.

In summary, the adhesion force between primary particles (Eq. (8)) increases lineally with R, while particle mass increases with the cubic power of R. Therefore, the relative stiffness and strength of particle chains decrease as R increases. Finally, larger primary particles leads to more poor mechanical properties of silica aerogels.

Relationship between tensile properties and density

In the work of Ma et al.,[14, 23] the modulus-density relationship was considered to be determined by the variation of structural connectivity with aerogel density. By contrast, in the work of Gelb et al.,[28] the modulus-density relationship was described by the variation of volumetric bond (neck) density with aerogel density. In the two work, primary particle size is considered to be unchanged with aerogel density. However, this assumption may be not reasonable, especially when aerogel density varies in a wide range. Therefore, it can be inferred that the power-law relationship between tensile properties and aerogel density may be affected by 'primary particle radius-density' relationship.

Some experimental results[30] have indicated the variation of primary particle radius with aerogel density; however, the precise 'primary particle radius-density'

20

relationship has not been reported. To solve the problem, we approximately obtain the

'primary particle radius-density' relationship based on the experimental data of

specific surface area and aerogel density. The procedures are described as follows: the

experimental data of aerogel density and the corresponding specific surface area are

cited from literature; the primary particle radius of each experimental sample is

calculated according to Eq.(1); the variation of primary particle radius with aerogel

density are obtained and illustrated in Fig. 9. As shown in Fig. 9, primary particle

radius in Exp. 1[45], Exp. 2[46], Exp. 3[47] and Exp. 4[48] changes significantly with aerogel

density, while primary particle radius in Exp. 5[49] and Exp. 7[50] is not observed to vary

evidently with density. R for the case of $\rho^* > 0.25$ is about 2nm in Exp. 5 while

the one is larger 3nm in Exp. 6[30] and Exp. 8[51]. On the whole, Fig. 1 shows a tendency

toward larger primary particles at higher aerogel density. In the following, two

methods are adopted to estimate the power-law relationship between tensile properties

and aerogel density.

Firstly, based on the results in Exp. 5 and Exp. 7 (Fig. 9), we assume that

primary particle radius does not vary with aerogel denisty. In this case, the power-law

relationship between tensile properties and aerogel density is only determined by

structural connectivity of microstructure. This hypothesis was also invoked to explain

the modulus-density relationship of silica aerogels by Ma *et al.*[14, 23] In this paper, four

types of numerical models are established, and their primary particle radiuses are 1nm,

1.5nm, 2nm and 3nm, respectively. According to Eq. (1), their specific surface areas

are about 1364, 909, 682 and 455 m^2/g, respectively. To ensure the reproducibility of

21

results, each reported result is from the mean value of 6 numerical samples in the following. The numerical results, obtained by the four types of numerical models, are shown in Fig. 10(a) for elastic modulus and in Fig. 10(b) for tensile strength, respectively. As show in Fig. 10(a), the predicted power-law exponents of modulus-density relationship are in the range of 3.84 to 3.91 for fixed particle radius. The difference among the four exponents is very slight and can even be neglected. Therefore, the power-law exponent of modulus-density relationship is approximately 3.88±0.03 if only the effect of structural connectivity is considered. Fig. 10(b) indicates the power-law exponents predicted by the four types of numerical models are in the range of 3.11 to 3.17 if R is unchanged with ρ^*. Similarly, the difference among the four predicted exponents can be neglected; therefore, the power-law exponent in 'tensile strength-density' relationship is taken as 3.14±0.03, provided that only structural connectivity of microstructure changes with density.

Secondly, we assume that primary particle radius changes with aerogel density. That is, the power-law relationship between tensile properties and density is determined by the variation of structural connectivity and size effects of primary particle. Based on the experimental results shown in Fig. 9, we propose a hypothetical relationship to describe the variation of primary particle radius with aerogel density, which is listed in Table 2. Fig. 9 indicates that the hypothetical relationship approximately describe the variation of primary particle radius with aerogel density. Next, some numerical results are picked from Fig.10 according to the hypothetical relationship between R and ρ^*. These selected numerical results are illustrated in

22

the insets of Fig. 10, and then fitted by power-law functions as well. After the variation of R with ρ^* is considered, the predicted exponents are 3.06 for the modulus-density relationship and 2.25 for the strength-density relationship, respectively. Clearly, the two power-law relationships are those incorporating the effects of structural connectivity and primary particle size.

Comparing the power-law exponents estimated by the two methods, we can conclude that the size effects of primary particle have significant influences on the power-law relationship of silica aerogels. The presently predicted exponents are compared with the experimental and other numerical results in literature as listed Table 3. The conclusions can be drawn based on the comparisons in Table 3 as follows. The power-law exponent in modulus-density relationship is 3.88 if the size effects of primary particle are not considered in our model. This value is close to the upper bound of experimental data (3.8[52], 4.2[53]). By contrast, the exponent in modulus-density relationship is 3.06 if the hypothetical relationship between particle size and aerogel density is incorporated. The corrected value is close to the lower bound of experimental data (2.97[54], 3.2[11]) and the numerical results of Murillo *et al.*[18] and Gelb *et al.*[27] Nevertheless, the variation of primary particle radius with aerogel density may be less evident than the hypothetical relationship (Fig. 9). Therefore, when the effects of structural connectivity and primary particle, the power-law exponents in the modulus-density relationship should be in the range of 3.06 to 3.88 for silica aerogels within a wide density range. Similarly, the power-law exponents in the strength-density relationship should be in the range of 2.25 to 3.14 for silica

aerogels within a wide density range, provided that both the variation of structural

connectivity and size effects of primary particle are considered. Clearly, the predicted

two exponent ranges almost cover the experimental results and other numerical results.

As shown in Table 3, the present results also explain the difference among

experimental exponents to a certain extent.

Furthermore, the quantitative comparisons between the present results and

experimental data[11] are shown in Fig. 10. Clearly, the numerical model with fixed

primary particle radius is insufficient to precisely predict the mechanical properties of

silica aerogels within such a wide density range. For example, the numerical model

with $R = 3\,nm$ well estimates experimental data for the case of $\rho^* > 0.25g/cm^3$

while the numerical models with $R = 2\,nm$ and $R = 1.5\,nm$ are more suitable for the

case of $0.1 < \rho^* < 0.25g/cm^3$. After the size effects of primary particle are

considered according to the hypothetical relationship in Table 2, the present results are

in good quantitative accordance with experimental data. In comparison with the

model of Murillo *et al.*,[18] the present two-level model provides a better quantitative

prediction of tensile strength. In particular, the present model is the only multi-scale

model which is used to estimate the strength properties of silica aerogels (Table 3).

In a word, the numerical models used for silica aerogels are still scarce. The

comparisons of the present results with experimental results and other numerical

results validate the present model. Consequently, this two-level model provides an

alternative theoretical-numerical approach to both the elastic and strength properties

of silica aerogels. Moreover, the present results indicate that the size effects of

24

primary particle are very important for the mechanical properties of silica aerogels with nanoporous structure. The similar size effects have been reported for other types of nanoporous materials.[55-57] For these nanoporous materials, a simple theoretical description based on conventional porous materials is not enough.

Conclusions

A two-level model based on sol-gel process is proposed to investigate the tensile properties of silica aerogels. This two-level model comprises the particle-particle interaction model and cluster structure model. The particle-particle interaction model describes the interactions between primary particles based on the polymerization reaction. In the particle-particle interaction model, the neck area between primary particles is obtained from theoretical derivations, which is related to the geometrical size and elastic properties of primary particles as well as the property of sol-gel solution. Based on interparticle neck size, the size-dependent interactions between primary particles are expressed as the short-range and long-range interactions. In the cluster structure model is generated based on a modified DLCA algorithm, and used to represent the microstructure of silica aerogels.

Based on DEM simulation, the tensile behavior of silica aerogels is determined by combining the particle-particle interaction model with the cluster structure model. The numerical results reveal extreme fragility of silica aerogels; a very low proportion of interparticle necks are fractured corresponding to the stress drop in the stress-strain curve. Moreover, the debonding particles are mostly between different clusters, and

25

almost lose one adjacent particle after brittle fracture occurs. The brittle fracture of

silica aerogels is found to be because the damage extends to the main framework of

the cluster structure. It can be inferred that the low cross-linked microstructure is

responsible for the poor mechanical properties of silica aerogels.

The numerical results show that the tensile properties of silica aerogels are

significantly dependent on primary particle size. As primary particle radius increases,

the relative neck radius as well as the relative stiffness and strength of particle chains

inversely decrease. Therefore, silica aerogels with larger primary particles have lower

elastic modulus and tensile strength. The power-law relationships between tensile

properties and density are obtained by four types of numerical models with different

particle radiuses. The predicted exponent in modulus-density relationship is around

3.88 when primary particle size does not change with aerogel density. A hypothetical

relationship is proposed to describe the variation of primary particle radius with

aerogel density based on experimental results in literature. The exponent in

modulus-density relationship is determined to be 3.06 according to the hypothetical

relationship between primary particle radius and aerogel density. Similarly, the

predicted exponent in strength-density relationship is about 3.14 for fixed primary

particle size, while the value is determined to be 2.25 based on the hypothetical

relationship. After both the variation of structural connectivity and size effects of

primary particle are considered, the power-law exponents should be in the range of

3.06 to 3.88 for the modulus-density relationship, and in the range of 2.25 to 3.14 for

the strength-density relationship, respectively, especially when aerogel density varies

26

in a wide range. The present results also explain the difference among experimental exponents to a certain extent. Moreover, this two-level model provides good quantitative estimations of the elastic modulus and tensile strength of silica aerogels after the size effects of primary particle are considered.

In a word, this two-level model provides an alternative theoretical-numerical approach to both the elastic and strength properties of silica aerogels. In particular, the investigation of the relationship between microstructure and mechanical properties indicates the size effects are very important for the mechanical properties of such nanoporous materials. Furthermore, the two-level model can be extended to study the mechanical properties of other aerogels and aerogel composites.

Acknowledgments

27

References

1. S. S. Kistler, *Nature*, 1931, **127**, 741.

2. N. Leventis, C. Sotiriou-Leventis, G. Zhang and A.-M. M. Rawashdeh, *Nano Lett.*, 2002, **2**, 957-960.

3. D. P. Mohite, S. Mahadik-Khanolkar, H. Luo, H. Lu, C. Sotiriou-Leventis and N. Leventis, *Soft Matter*, 2013, **9**, 1531-1539.

4. A. C. Pierre and G. M. Pajonk, *Chem. Rev.*, 2002, **102**, 4243-4266.

5. T. Y. Wei, T. F. Chang, S. Y. Lu and Y. C. Chang, *J. Am. Ceram. Soc.*, 2007, **90**, 2003-2007.

6. D. P. Mohite, Z. J. Larimore, H. Lu, J. T. Mang, C. Sotiriou-Leventis and N. Leventis, *Chem. Mater.*, 2012, **24**, 3434-3448.

7. M. A. Aegerter, N. Leventis and M. M. Koebel, *Aerogels handbook*, Springer, New York, 2011.

8. D. W. Schaefer and K. D. Keefer, *Phys. Rev. Lett.*, 1986, **56**, 2199-2202.

9. J. Mrowiec-Bialon, L. Pajak, A. B. Jarzebski, A. I. Lachowski and J. J. Malinowski, *Langmuir*, 1997, **13**, 6310-6314.

10. L. J. Gibson and M. F. Ashby, *Cellular solids: structure and properties*, Cambridge university press, 1999.

11. T. Woignier, J. Reynes, A. Hafidi Alaoui, I. Beurroies and J. Phalippou, *J. Non-Cryst. Solids*, 1998, **241**, 45-52.

12. J. Gross, T. Schlief and J. Fricke, *Mater. Sci. Eng., A*, 1993, **168**, 235-238.

13. M. Moner-Girona, A. Roig, E. Molins and J. Esteve, *Appl. Phys. Lett.*, 1999, **75**, 653-655.

14. H.-S. Ma, A. P. Roberts, J.-H. Prévost, R. Jullien and G. W. Scherer, *J. Non-Cryst. Solids*, 2000, **277**, 127-141.

15. J. Kieffer and C. A. Angell, *J. Non-Cryst. Solids*, 1988, **106**, 336-342.

16. A. Nakano, L. Bi, R. K. Kalia and P. Vashishta, *Phys. Rev. Lett.*, 1993, **71**, 85.

17. J. M. Rimsza and J. Du, *J. Am. Ceram. Soc.*, 2013.

18. J. S. Rivas Murillo, M. E. Bachlechner, F. A. Campo and E. J. Barbero, *J. Non-Cryst. Solids*, 2010, **356**, 1325-1331.

19. J.-J. Zhao, Y.-Y. Duan, X.-D. Wang and B.-X. Wang, *J. Phys. D: Appl. Phys.*, 2013, **46**,

015304.

20.   L. D. Gelb, in *Aerogels Handbook*, Springer, 2011, pp. 565-581.

21.   F. A. Campo, J. S. Murillo and E. J. Barbero, *J. Non-Cryst. Solids*, 2011, **357**, 2046-2053.

22.   A. Hasmy, E. Anglaret, M. Foret, J. Pelous and R. Jullien, *Phys. Rev. B*, 1994, **50**, 6006.

23.   H.-S. Ma, J.-H. Prévost and G. W. Scherer, *Int. J. Solids. Struct*, 2002, **39**, 4605-4614.

24.   H.-S. Ma, R. Jullien and G. W. Scherer, *Phys. Rev. E*, 2002, **65**, 041403.

25.   E. J. Barbero and F. A. Campo, *J. Non-Cryst. Solids*, 2012, **358**, 728-734.

26.   L. D. Gelb, *J. Phys. Chem. C*, 2007, **111**, 15792-15802.

27.   C. A. Ferreiro-Rangel and L. D. Gelb, *J. Phys. Chem. B*, 2013.

28.   J. Lei, Z. Liu, J. Yeo and T. Y. Ng, *Soft Matter*, 2013, **9**, 11367-11373.

29.   R. K. Iler, *The chemistry of silica: solubility, polymerization, colloid and surface properties, and biochemistry*, John Wiley & Sons, New York, 1979.

30.   T. Woignier and J. Phalippou, *J. Non-Cryst. Solids*, 1988, **100**, 404-408.

31.   U. D. Schwarz, *J. Colloid Interface Sci.*, 2003, **261**, 99-106.

32.   K. L. Johnson, K. Kendall and A. D. Roberts, *Proc. R. Soc. London, Ser. A*, 1971, **324**, 301-313.

33.   T. Tsuru and Y. Shibutani, *Phys. Rev. B*, 2007, **75**, 035415.

34.   G. Ziegenhain, A. Hartmaier and H. M. Urbassek, *J. Mech. Phys. Solids*, 2009, **57**, 1514-1526.

35.   D. S. Grierson, J. Liu, R. W. Carpick and K. T. Turner, *J. Mech. Phys. Solids*, 2012.

36.   G. Jefferson, G. K. Haritos and R. M. McMeeking, *J. Mech. Phys. Solids*, 2002, **50**, 2539-2575.

37.   D. Jauffrès, C. L. Martin, A. Lichtner and R. K. Bordia, *Modell. Simul. Mater. Sci. Eng.*, 2012, **20**, 045009.

38.   A. Balakrishnan, P. Pizette, C. L. Martin, S. V. Joshi and B. P. Saha, *Acta Mater.*, 2010, **58**, 802-812.

39.   D. Jauffrès, C. L. Martin, A. Lichtner and R. K. Bordia, *Acta Mater.*, 2012, **60**, 4685-4694.

40.   P. U. Manual, *PFC3D, version 3.1*, Itasca Consulting Group Inc., USA, 2004.

41.   I. Ostanin, R. Ballarini, D. Potyondy and T. Dumitrică, *J. Mech. Phys. Solids*, 2013, **61**, 762-782.

42.   S. Leroch and M. Wendland, *J. Phys. Chem. C*, 2012, **116**, 26247-26261.

43.   P. Brommer, P. Beck, A. Chatzopoulos, F. Gähler, J. Roth and H.-R. Trebin, *J. Chem. Phys.*, 2010, **132**, 194109.

44.   T. Frolov and Y. Mishin, *Phys. Rev. B*, 2009, **79**, 045430.

45.   P. B. Sarawade, J.-K. Kim, H.-K. Kim and H.-T. Kim, *Appl. Surf. Sci.*, 2007, **254**, 574-579.

46.   A. Hilonga, J.-K. Kim, P. B. Sarawade and H. T. Kim, *J. Alloys Compd.*, 2009, **487**, 744-750.

47.   M. Alnaief and I. Smirnova, *J. Non-Cryst. Solids*, 2010, **356**, 1644-1649.

48.   L.-J. Wang, S.-Y. Zhao and M. Yang, *Mater. Chem. Phys.*, 2009, **113**, 485-490.

49.   S. D. Bhagat, Y.-H. Kim, K.-H. Suh, Y.-S. Ahn, J.-G. Yeo and J.-H. Han, *Microporous Mesoporous Mater.*, 2008, **112**, 504-509.

50.   J. C. Wong, H. Kaymak, S. Brunner and M. M. Koebel, *Microporous Mesoporous Mater.*, 2014, **183**, 23-29.

51.   J. Phalippou, T. Woignier and M. Prassas, *J Mater. Sci.*, 1990, **25**, 3111-3117.

52.   T. Woignier, J. Pelous, J. Phalippou, R. Vacher and E. Courtens, *J. Non-Cryst. Solids*, 1987, **95**, 1197-1202.

53.   A. H. Alaoui, T. Woignier, G. W. Scherer and J. Phalippou, *J. Non-Cryst. Solids*, 2008, **354**, 4556-4561.

54.   J. Groβ and J. Fricke, *Nanostruct. Mater.*, 1995, **6**, 905-908.

55.   L. Zixing, Z. Cungang, L. Qiang and Y. Zhenyu, *J. Phys. D: Appl. Phys.*, 2011, **44**, 395404.

56.   Z. Lu, M. Zhu and Q. Liu, *J. Phys. D: Appl. Phys.*, 2014, **47**, 065310.

57.   X.-Q. Feng, R. Xia, X. Li and B. Li, *Appl. Phys. Lett.*, 2009, **94**, 011916.

58.   T. Campbell, R. K. Kalia, A. Nakano, F. Shimojo, K. Tsuruta, P. Vashishta and S. Ogata, *Phys. Rev. Lett.*, 1999, **82**, 4018.

59.   G. W. Scherer, D. M. Smith, X. Qiu and J. M. Anderson, *J. Non-Cryst. Solids*, 1995, **186**, 316-320.

Figures
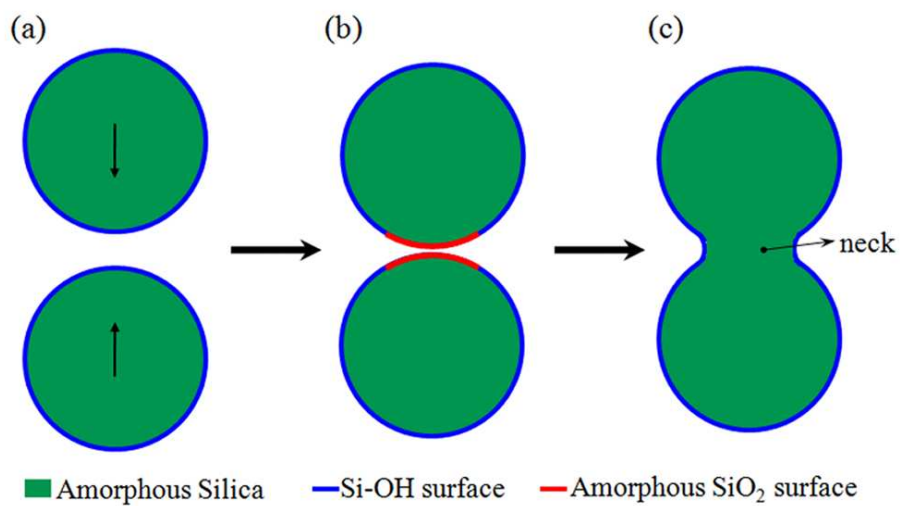
Fig. 1. The formation of interparticle neck.
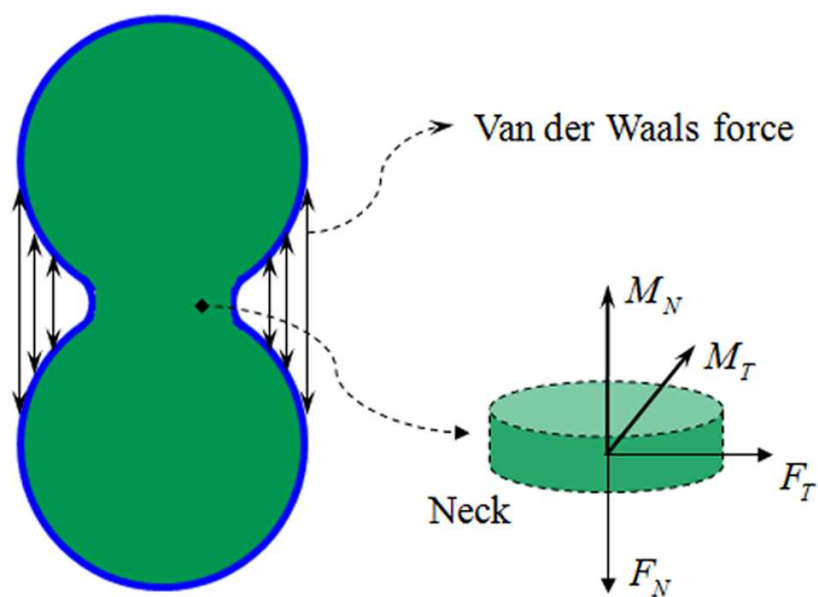
Fig. 2. The interactions between primary particles.

31
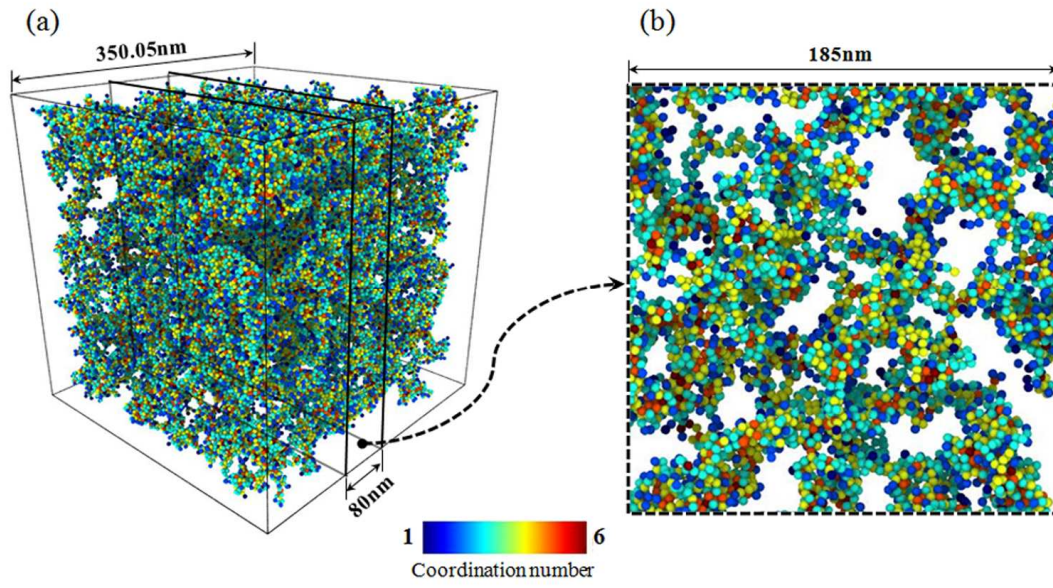
Fig. 3. The generated cluster structure colored by the coordination number: (a) the overall structure and

(b) the local structure of zoom lens.
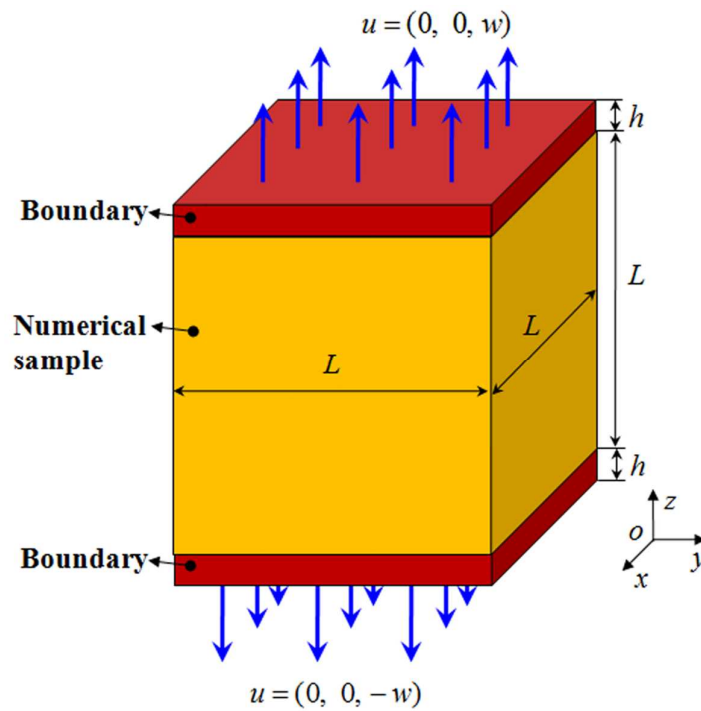
Fig. 4. The schematic diagram of numerical sample under tension.
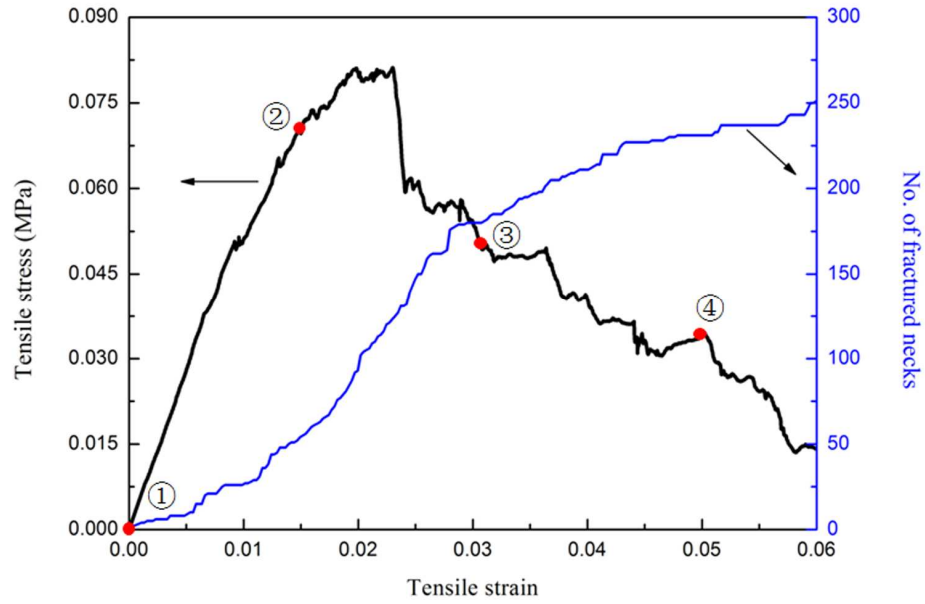
Fig. 5. The simulated stress-strain response of the silica aerogel with density of $0.12 g/cm^3$.
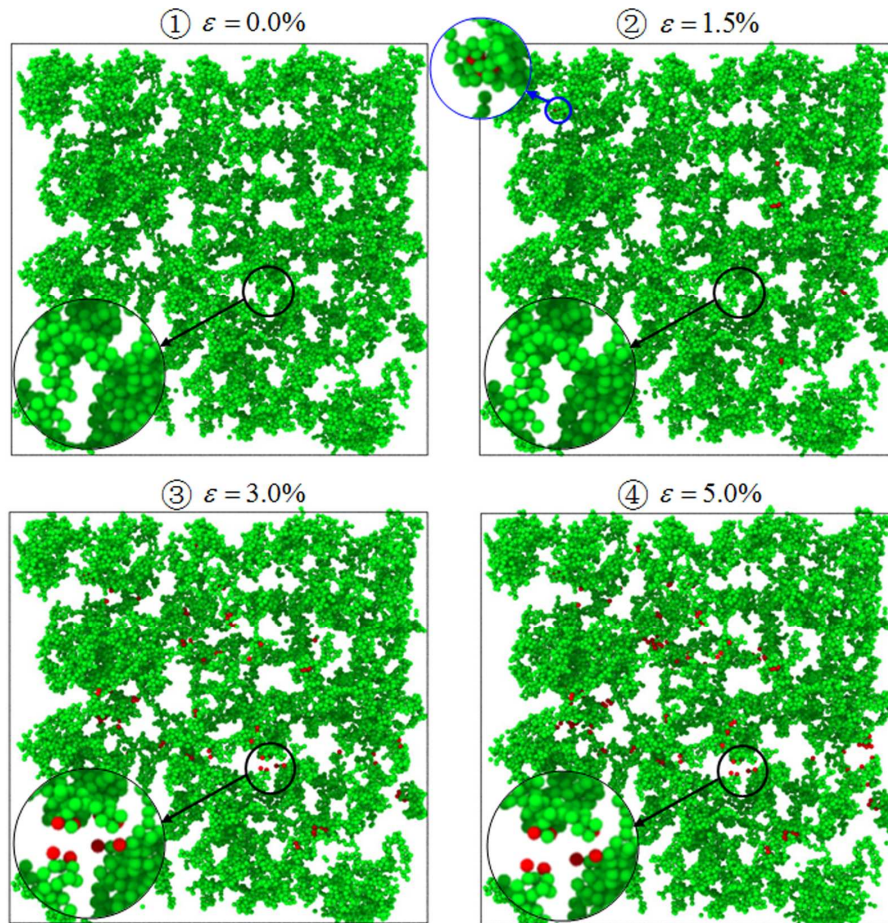
Fig. 6. The microstructure evolution of the silica aerogel under tension corresponding to Fig. 5.

33
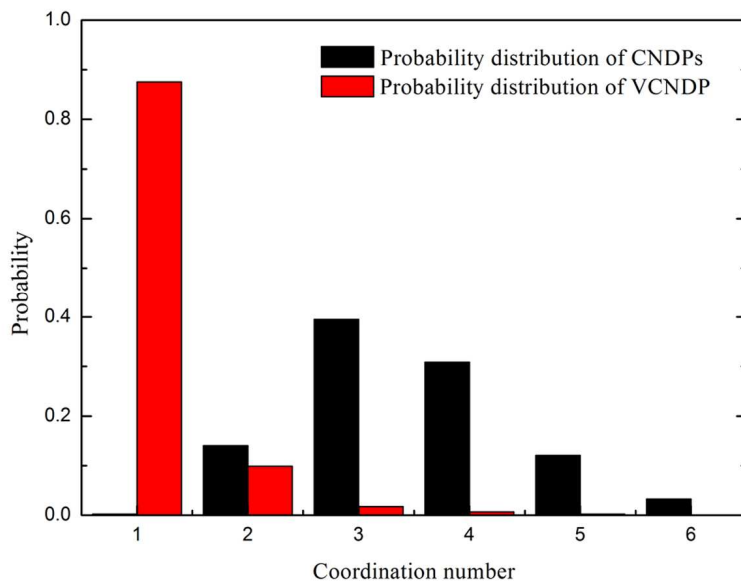
Fig. 7. The probability distribution of CNDPs and VCNDP.
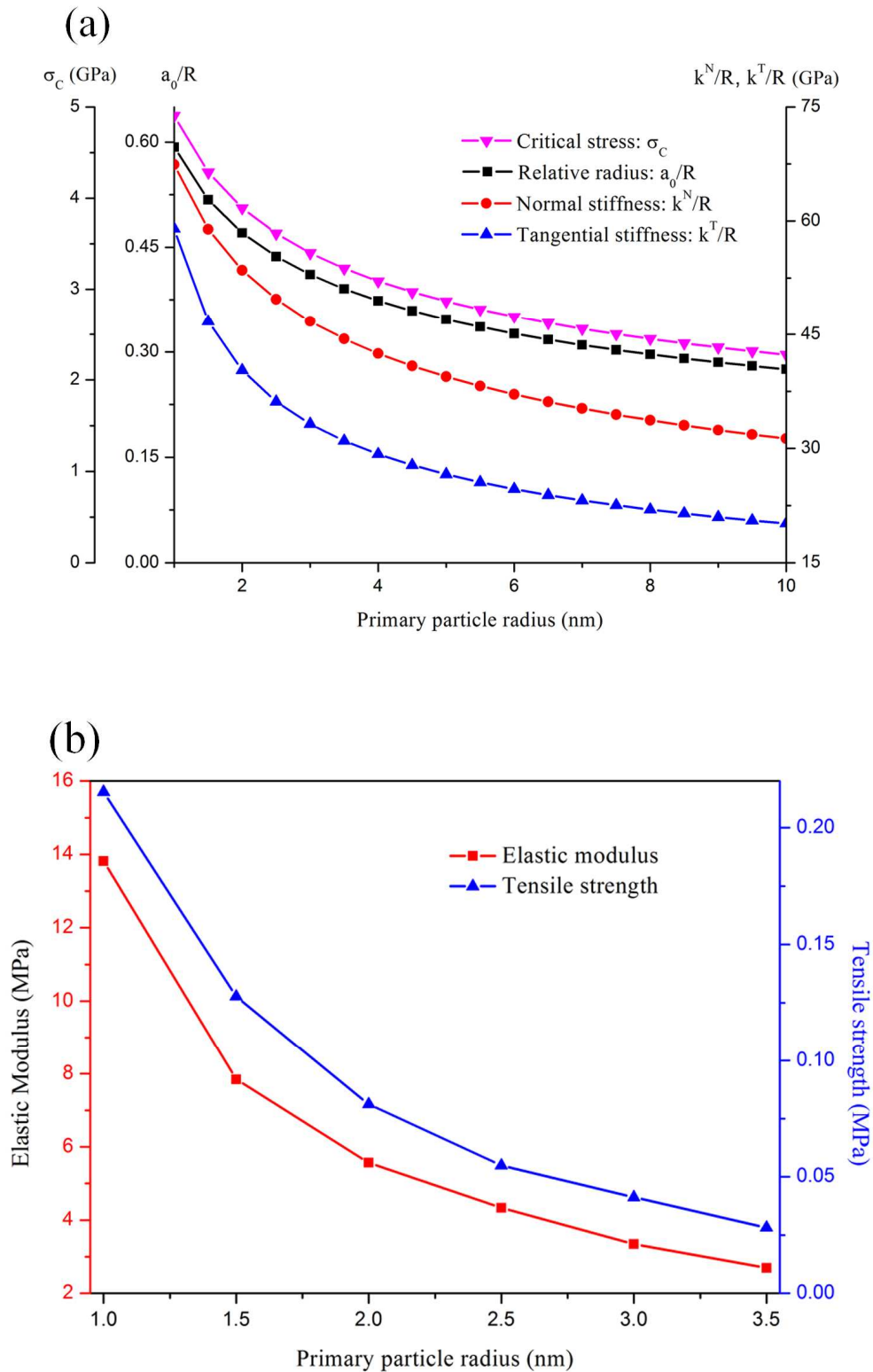
Fig. 8. (a) The size-dependent properties of interparticle neck, (b) The effects of primary particle size

on the tensile properties of silica aerogels.
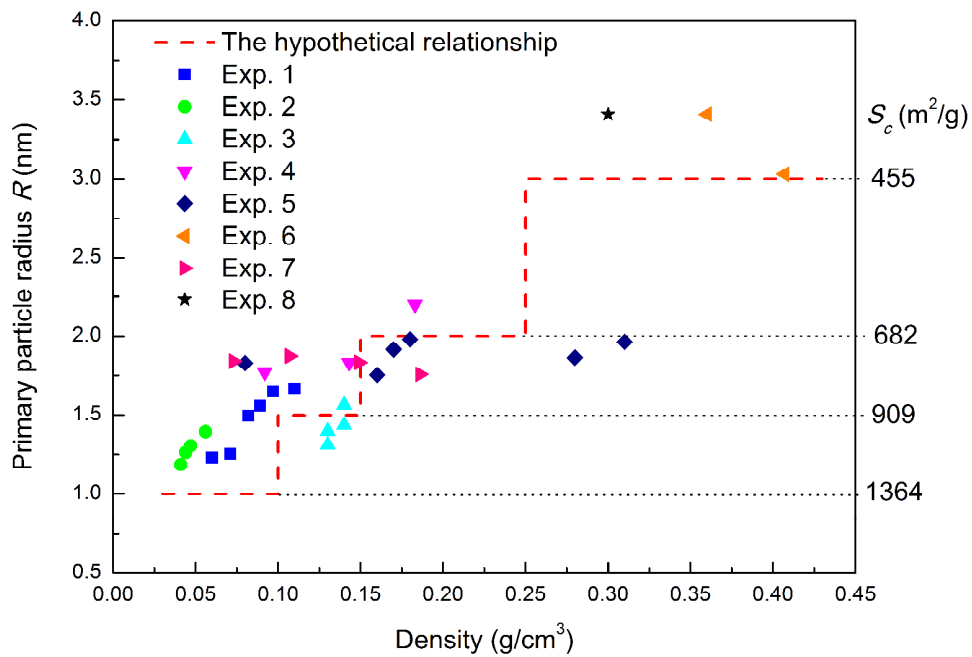
Fig. 9 The variation of primary particle radius with aerogel density.

(a)

(b)
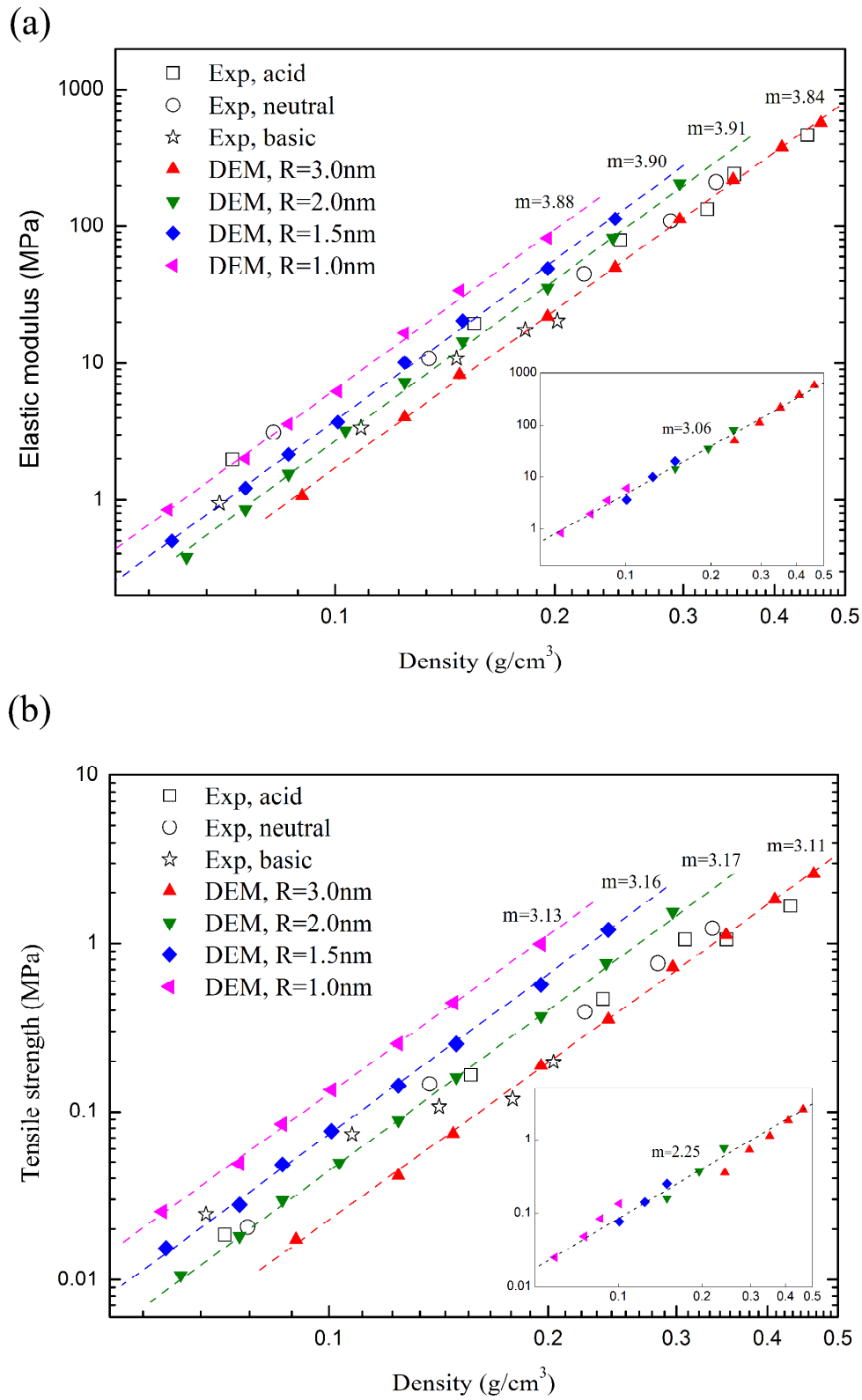
Fig. 10. The size-dependent power-law relationships between (a) elastic modulus and density (b) tensile strength and density obtained by DEM simulation.

37

Table

Table 1 The material parameters and model parameters.

E_0	μ_0	γ_{SiO_2}	γ_{Si-OH}^{liquid}	γ_{Si-OH}^{air}
72.56GPa	0.17	1.14 J/m^2	0.112 J/m^2	0.027 J/m^2

Table 2 The hypothetical relationship between primary particle radius and aerogel density based on the experimental results in Fig. 9.

Density ρ^* (g/cm^3)	Primary particle radius R (nm)
$\rho^* \leq 0.1$	1
$0.1 < \rho^* < 0.15$	1.5
$0.15 \leq \rho^* < 0.25$	2
$\rho^* \geq 0.25$	3

38

Table 3   The comparisons of the present results with the experimental and other

numerical results in the literature.

Reference	Power-law exponent in modulus-density relationship	Power-law exponent in strength-density relationship	Density (g/cm^3)	Descriptions
Groβ et al[54]	3.49±0.07	-	0.14~2.7	Experiment
	2.97±0.05	-	0.08~1.2	Experiment
Scherer et al[59]	≈3.6	-	0.0675~0.188	Experiment
Woignier et al[11, 52, 53]	3.8±0.2	-	≈0.1~0.4	Experiment[52]
	3.7±0.2	2.6±0.2	≈0.055~0.5	Experiment[11]
	3.2±0.2	2.3±0.2	≈0.42~2.2	Experiment[11]
	4.2±0.1	-	0.09~0.25	Experiment[53]
Wong et al[50]	3.62±0.05	2.33±0.05	≈0.05~0.35	Experiment
Campbell et al[58]	3.5±0.2	-	1.67~2.2	Atomistic model
Murillo et al[18]	3.11±0.21	2.53±0.15	0.23~2.2	Atomistic model
Rimsza and Du[17]	2.27, 2.8	-	0.22~1.54	Atomistic model
Ma et al[23]	3.6±0.2	-	0.018~0.18	Finite element model
Lei et al[28]	3.168	-	0.5~1.1	Multi-scale model
Gelb et al[27]	3.03~3.14	-	≈0.05~0.24	Multi-scale model
This paper	3.06~3.88	2.25~3.14	0.05~0.5	Multi-scale model

• '-' means that the data is not available.